Li$_2$SiO$_3$ Coating to Improve the High-voltage Performance of LiNi$_{1/3}$Co$_{1/3}$Mn$_{1/3}$O$_2$ Cathode

Jianfu He[1,2], Xiaodong Chu[1],Yan-Bing He[1], Dongqing Liu[1], Yuxiu Liu[1,2], Junxiong Wu[1,2], Baohua Li[1*], and Feiyu Kang[2,2]

[1] Engineering Laboratory for Next Generation Power and Energy Storage Batteries, Graduate School at Shenzhen, Tsinghua University, Shenzhen 518055, China.
[2] School of Materials Science and Engineering, Tsinghua University, Beijing 100084, China.
[*]E-mail: libh@mail.sz.tsinghua.edu.cn

The poor high voltage performance of LiNi$_{1/3}$Co$_{1/3}$Mn$_{1/3}$O$_2$ (NCM) materials has become a main challenge for its practical application towards electric vehicles (EV). In this work, we develop a novel method to synthesize Li$_2$SiO$_3$-coated NCM cathode material and systematically investigate its high-voltage performance at 4.5 V. The results show that the Li$_2$SiO$_3$ coating layer cannot only prevent the cation disorder of the layered structure but also alleviate the interfacial reaction between the cathode and the electrolyte, leading to reduction of the charge transfer resistance and improvement of the kinetic performance. This cathode exhibits a capacity retention of 80.0 % after 200 cycles at room temperature and 87.6 % after 100 cycles at 45 °C, while the corresponding values of bare NCM are only 62.1 % and 81.4 %, respectively. In addition, the discharge specific capacities of Li$_2$SiO$_3$ coated NCM cathode at 2 C and 10 C could reach 154.4 and 104.4 mAh g^{-1}, respectively.

1. INTRODUCTION

With the increasing demand for clean and efficient energy, lithium-ion batteries (LIBs) are thought to be an ideal energy source due to their significantly higher energy density than other energy storage devices [1]. Cathode as a major component of LIBs plays an significant role in battery cycling life, safety and energy density of LIBs. However, since lithium cobalt oxide (LiCoO$_2$) has relatively low capacity, poor cycling, high cost and environmental toxicity, it cannot completely meet the real requirements of LIBs with higher energy density [2]. Therefore, the development of environmentally-friendly and low-cost cathode materials with higher capacity and better cycling properties is highly

demanded.

$LiNi_{1/3}Co_{1/3}Mn_{1/3}O_2$ (NCM) with high specific capacity and low-cost has been considered as a suitable cathode material for energy storage devices in electric vehicles (EV). Nevertheless, there are still some problems associated with NCM, such as poor cycling and rate capacity, which will at high voltage because of serious side reactions between the NCM and electrolyte [2, 3]. Researchers have proposed various ways to improve the electrochemical performance of NCM. For example, constructing new and well-controlled morphologies, including nanobricks [4], nanoflowers [5, 6], hollow nano-micro hierarchical microspheres [7], 3-D dumbbell-like [8], 1-D hierarchical microrods [9, 10] and tuning surface structure to expose more active crystal faces [11-13]. Aside from this, the addition of a protective coating layer on NCM is also beneficial as it can prevent the direct contact between the active materials and the electrolyte, therefore suppressing the side reactions between them [14]. Metal oxides (TiO_2 [3, 15], CeO_2 [16]) and carbon [17, 18] have been used as coating materials for NCM due to their capability to reduce charge transfer resistance as well as to restrain the side reactions between the electrolyte and the active materials. Although the coating materials could enhance the cycling performance by improving the structure stability, the rate capability may be hindered by the surface coating layers due to their lower lithium-ion diffusion coefficient (D_{Li}).

Li_2SiO_3 with 3D lithium-ion diffusion path is considered to be an ideal coating material for NCM. As a chemically inert material in organic electrolyte, Li_2SiO_3 can guarantee structural stability, which plays a crucial role in both protecting the surface of NCM and increasing the diffusion rate of lithium ion [21]. Recently, Zhao et al reported that the addition of Li_2SiO_3 coating layer could significantly improve the electrochemical performance of $Li_{1.13}Ni_{0.03}Mn_{0.57}O_2$ [22]. The enhanced electrochemical performance was attributed to the SiO_4 tetrahedra in Li_2SiO_3, which effectively inhibited the hydrofluoric acid (HF) erosion in the electrolyte at high-voltages above 4.5 V.

In this work, we utilized the inherent advantages of Li_2SiO_3 such as its inactive properties in electrolyte and high D_{Li} to improve the high voltage cycling and rate performance of NCM at high temperatures. The uniform Li_2SiO_3 coating layer on NCM was achieved via hydrolysis reaction and solid state method. The Li_2SiO_3 coated NCM exhibits excellent performance at both room and elevated temperatures at a high voltage of 4.5 V. For instance, the Li_2SiO_3-coated NCM exhibits a capacity retention of 80.0 % after 200 cycles at room temperature and 87.6 % after 100 cycles at 45 °C, and the corresponding values of the bare NCM are only 62.1 % and 81.4 %, respectively. In addition, the Li_2SiO_3 coated NCM shows a much better rate performance with specific capacities of 154.4 and 104.4 mAh g^{-1}, compared to the bare NCM with lower specific capacities of 141.8 and 89.8 mAh g^{-1} at 2 C and 10 C, respectively.

2. EXPERIMENTAL

2.1 Synthesis of Li_2SiO_3 coated $LiNi_{1/3}Co_{1/3}Mn_{1/3}O_2$

Co-precipitation method was adopted to obtain $Ni_{1/3}Co_{1/3}Mn_{1/3}(OH)_2$ precursor and an inert gas (N_2) was injected into the reaction vessel to prevent the precursor from being oxidized. To achieve a

concentration of 1.0 mol/L solution, $NiSO_4 \cdot 6H_2O$, $CoSO_4 \cdot 7H_2O$, and $MnSO_4 \cdot H_2O$ (metal ions ratio of Ni:Co:Mn=1:1:1) were dissolved in 300 mL deionized water and stirred well to fully dissolve the above compounds. Meanwhile, NaOH solution (2 M) was mixed with a proper amount of NH_4OH dripped into a reactor via peristaltic pump under nitrogen atmosphere. The chemical reaction lasted up to 6 hours to obtain $Ni_{1/3}Co_{1/3}Mn_{1/3}(OH)_2$ slurry and the slurry was aged for 24 hours. The obtained slurry was subsequently washed with deionized water for several times to remove impurity ions and then dried at 110 °C under vacuum. The $Ni_{1/3}Co_{1/3}Mn_{1/3}(OH)_2$ was then dispersed into a mixture of 20 mL absolute ethanol, 200 μL NH_4OH and 2 mL deionized water as solution A. A calculated amount of $Si(OC_2H_5)_4$ was dissolved in 60 mL absolute ethanol as solution B. Next, solution A was swiftly poured into solution B and the mixed solution was stirred at 50 °C for 6 hours. The obtained product was washed with ethanol and dried at 110 °C under vacuum overnight to get $SiO_2@Ni_{1/3}Co_{1/3}Mn_{1/3}(OH)_2$ powders. To achieve the Li_2SiO_3-coated $LiNi_{1/3}Co_{1/3}Mn_{1/3}O_2$ (named as C-NCM), stoichiometric of $SiO_2@Ni_{1/3}Co_{1/3}Mn_{1/3}(OH)_2$ precursor and 5 wt. % excess $LiOH \cdot H_2O$ was ground for 3 h under an infrared lamp and was subsequently sintered at 450 °C for 9 h and at 900 °C for 12 h in air with a heating rate of 5 °C/min. The key chemical reactions can be described as follows:

$$Si(OC_2H_5)_4 + H_2O \longrightarrow SiO_2 + C_2H_5OH \qquad (1)$$

$$SiO_2@Ni_{1/3}Co_{1/3}Mn_{1/3}(OH)_2 + LiOH \cdot H_2O \longrightarrow Li_2SiO_3@LiNi_{1/3}Co_{1/3}Mn_{1/3}O_2 + H_2O \qquad (2)$$
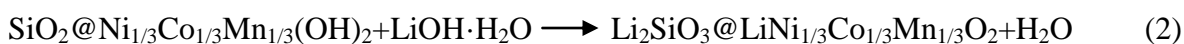
The pure $LiNi_{1/3}Co_{1/3}Mn_{1/3}O_2$ (named as B-NCM) was synthesized by a similar method without using $Si(OC_2H_5)_4$. The whole synthetic process of bare and coated $LiNi_{1/3}Co_{1/3}Mn_{1/3}O_2$ is schematically shown in Fig. 1.
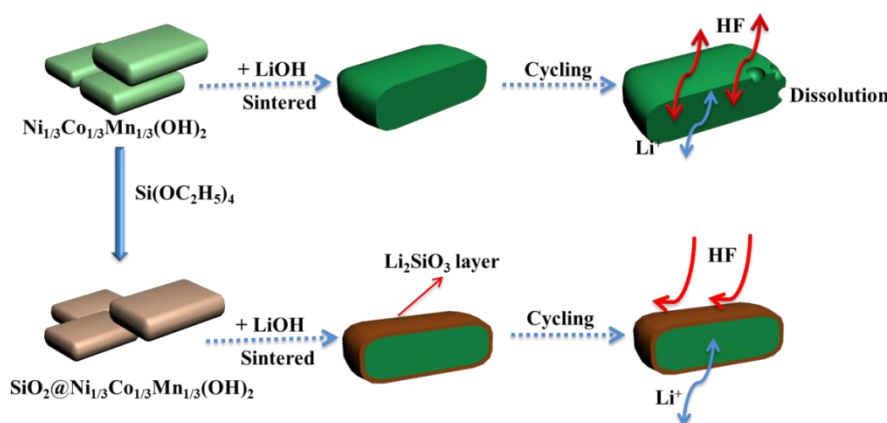
Figure 1. Schematic diagram of the synthetic process of the bare and Li_2SiO_3-coated $LiNi_{1/3}Co_{1/3}Mn_{1/3}O_2$.

2.2 Structural characterization

X-ray diffraction (XRD, Rigaku Dmax2500) was employed to examine the composition of B-NCM and C-NCM. The morphology of both bare and coated NCM particles was observed by scanning electron microscopy (SEM, Hitachi S-4800). The lattice information and crystal structure were examined using high-resolution transmission electron microscopy (HR-TEM, FEI G2 spirit) and

energy dispersive spectroscopy (EDS) adhered to the HR-TEM. X-ray photoelectron spectroscopy (XPS) measurement (ESCALAB 250Xi) was implemented to analyze the chemical species and states of the coating layer on the surface of NCM. To provide more evidence of the existence of the Li_2SiO_3 coating layer, Fourier transformation infrared spectroscopy (Bruker Vertex-70 spectrophotometer) and Raman spectroscopy (Labram HR800 Evolution) were used to examine the surface composition of the samples.

2.3 Electrochemical characterization

The electrochemical performance of the B-NCM and C-NCM was evaluated with CR2032-type coin cells and a glove box with lower than 1 ppm O_2 and 1 ppm water was used to assemble the coin cells. The cathode slurry, consisting of the as prepared active material, polyvinylidene fluoride and carbon black (weight ratio: 8:1:1), was adequately mixed and then tiled by film applicator. Liquid electrolyte, which includes 1M $LiPF_6$ adding ethylene carbonate, ethylene methyl carbonate, and dimethyl carbonate (volume ratio: 1:1:1), was injected on both sides of the polypropylene film by needle tube.

The rate performance of the coin cells were carried out with a LAND-CT 2001 battery tester at various rates ranging from 0.2 C to 10 C (The current density of 1 C is 170 mA g^{-1}). The cycling performance and capacity retention at 1C were also measured at room temperature and 45 °C. Biochemical incubator was used to provide a constant temperature. Cyclic voltammetry (CV) and electrochemical impedance spectroscopy (EIS) of the B-NCM and C-NCM cells were carried out using an electrochemical workstation (VMP3, Bio-Logic). The CV curves were swept between 2.5 V and 4.5 V vs. Li^+/Li at a scan rate of 0.1 mV s^{-1}. The EIS was conducted after the cells underwent 200 cycles at room temperature in the frequency range of100 kHz to 0.01 Hz with an amplitude of 5 mV.

3. RESULTS AND DISCUSSION

3.1 Structure and morphology

Fig. 2 shows the XRD patterns of the B-NCM and C-NCM samples. It can be observed that all the diffraction peaks correspond to layered α-$NaFeO_2$ structures with space group R-3m [20] and no impurity phase belongs to Li_2SiO_3 was identified. This suggests that the addition of Li_2SiO_3 does not influence the original structure of NCM. The apparent splitting of peaks (006)/(102) and (108)/(110) are observed in both samples suggesting a well ordered layered structure [6]. It is well-known that the intensity ratio of I_{003}/I_{104} is related to the degree of cation mixing and a high degree of cation mixing implies a barrier for Li^+ diffusion. When this value is larger than 1.2, it corresponds to a lower degree of cation mixing [21]. By calculating the data in Fig. 2, the I_{003}/I_{104} value of the C-NCM sample is 1.44, which is larger than that of the B-NCM (1.35), indicating a high D_{Li} of C-NCM.
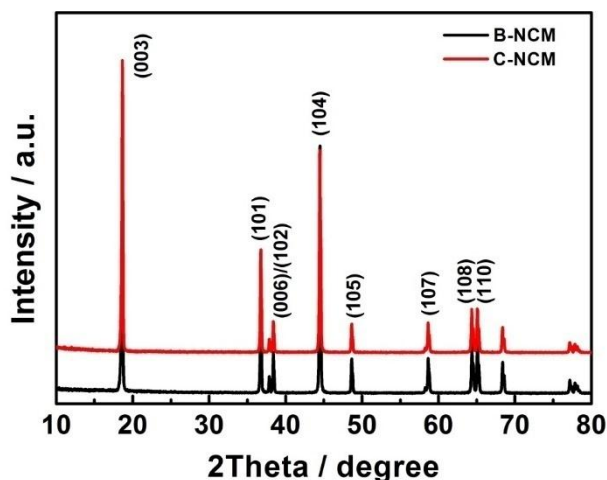
Figure 2. XRD patterns of the B-NCM and C-NCM samples.

The morphology of B-NCM and C-NCM were further characterized with SEM and TEM. As shown in Fig. 3, both samples exhibit similar morphology in the form of irregular lamella and the size of particle is about 200~400 nm. Furthermore, after the addition of Li_2SiO_3 coating layer, the morphology of C-NCM sample has negligible difference compared with B-NCM, indicating that the coating layer did not drastically change the morphology of NCM during the heat treatments.
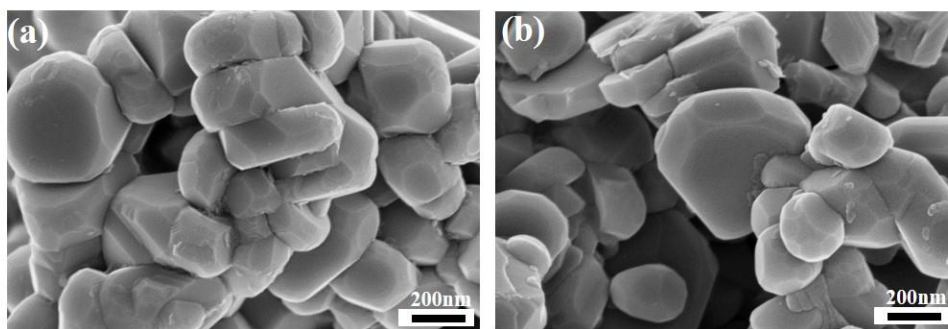
Figure 3. SEM images of the B-NCM (a) and C-NCM (b) samples.

Fig. 4(a, b, c, d) display the HR-TEM images of B-NCM and C-NCM samples. The lattice spacings of 0.475 nm and 0.143 nm are assigned to (003) and (110) planes of NCM, respectively. In Fig. 4(a, b), particles without coating layer have a clear edge and lattice spacing. In comparison, an obvious coating layer on the surface of NCM can be observed (~10 nm in thickness) in Fig. 4(c, d). The composition and elemental distribution of C-NCM were detected by EDS (Fig. 4e). It can be observed that nickel, cobalt, manganese, oxygen and silicon elements were well-distributed on the C-NCM particles. From the HR-TEM and EDS analysis, it can be deduced that the Li_2SiO_3 coating layer was uniformly coated on the surface of the C-NCM particles and had a compact contact with the bare NCM particles.
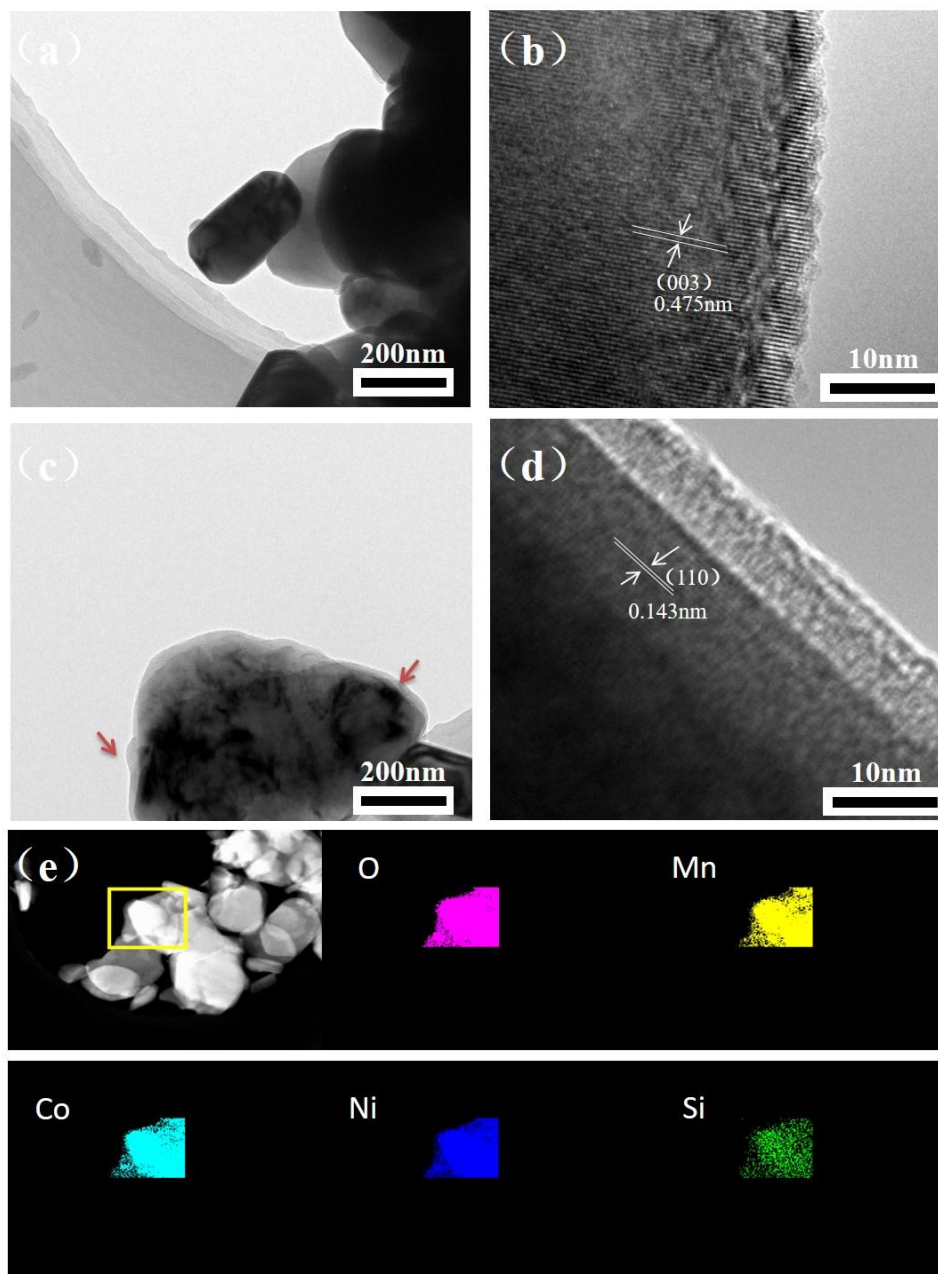
Figure 4. (a, b, c, d) HR-TEM images of the B-NCM and C-NCM samples. (e) Elemental mappings of O, Mn, Co, Ni Si, of the C-NCM particle.

Fig. 5a shows the FTIR spectra of the B-NCM and C-NCM samples. Compared with B-NCM, the FTIR spectra of C-NCM have a much broader peak at 1050~1100 cm^{-1} which is due to the stretching vibration at 1060~1070 cm^{-1}of O-Si-O and an absorption band is observed at around 880 cm^{-1}, which corresponds to Li$_2$SiO$_3$ [22]. The Raman spectra from 200-1500 cm^{-1} of the B-NCM and C-NCM samples are shown in Fig. 5b. Abroad vibration at 535~650 cm^{-1} corresponding to metal oxides (Ni-O, Co-O, Mn-O) was observed in both samples. Moreover, the vibration at 835 cm^{-1} is indexed to Si-O-Si [23]. Based on the FTIR and Raman results, it can be proven that Li$_2$SiO$_3$ was successfully coated on the surface of LiNi$_{1/3}$Co$_{1/3}$Mn$_{1/3}$O$_2$.
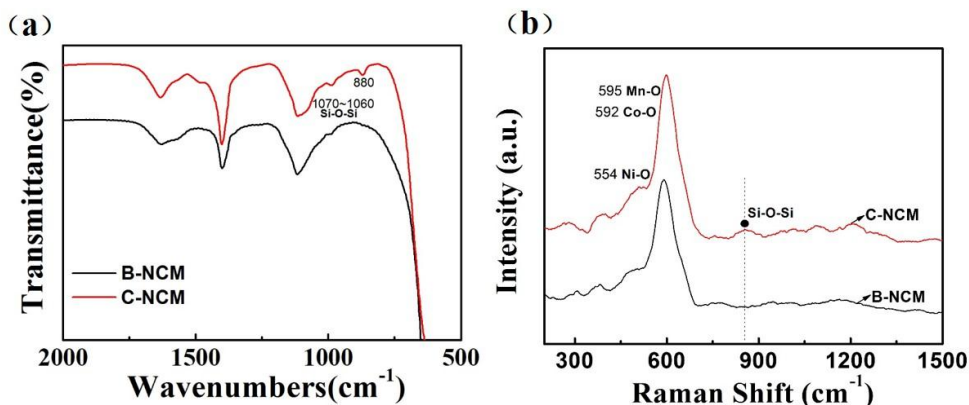
Figure 5. (a) FTIR spectra and (b) Raman spectra of B-NCM and C-NCM samples.

XPS analysis was used to examine the detailed chemical composition of the C-NCM surface, as shown in Fig. 6. In Fig. 6a, two characteristic peaks at binding energies of 854.6 and 872.2 eV corresponding to Ni^{2+} were observed. In addition, two shake-up satellite peaks at 860.9 (S1) and 878.9 (S2) eV are also observed, ascribed to the multiple splitting of energy levels in NiO [11, 21, 24]. It can be seen from Fig. 6b that two characteristic peaks exist at 779.9 and 794.9 eV, assigned to Co^{3+} and two low-intensity satellite peaks at 789.6 (S1) and 804.7 (S2) eV are also identified [11, 24]. Furthermore, in the Mn XPS spectra of C-NCM, the peak located at 642.1 eV corresponds well to Mn^{4+} [11, 24].
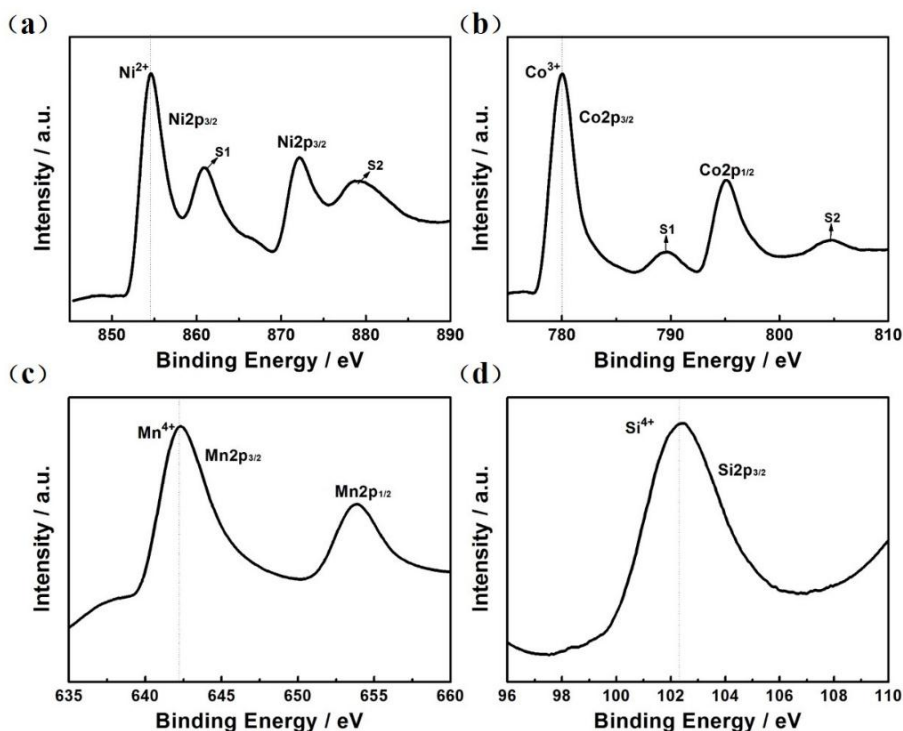
Figure 6. XPS spectra of the C-NCM sample. a) Ni2p, b) Co2p, c) Mn2p and d) Si2p.

Moreover, in Fig. 6d the binding energy of Si $2p_{3/2}$ at 102.0 eV is attributed to Si^{4+}, suggesting the existence of Li_2SiO_3 on the surface of C-NCM [19]. The above results provide evidence of the existence of Li_2SiO_3 on the surface of $LiNi_{1/3}Co_{1/3}Mn_{1/3}O_2$.

3.2 Electrochemical properties
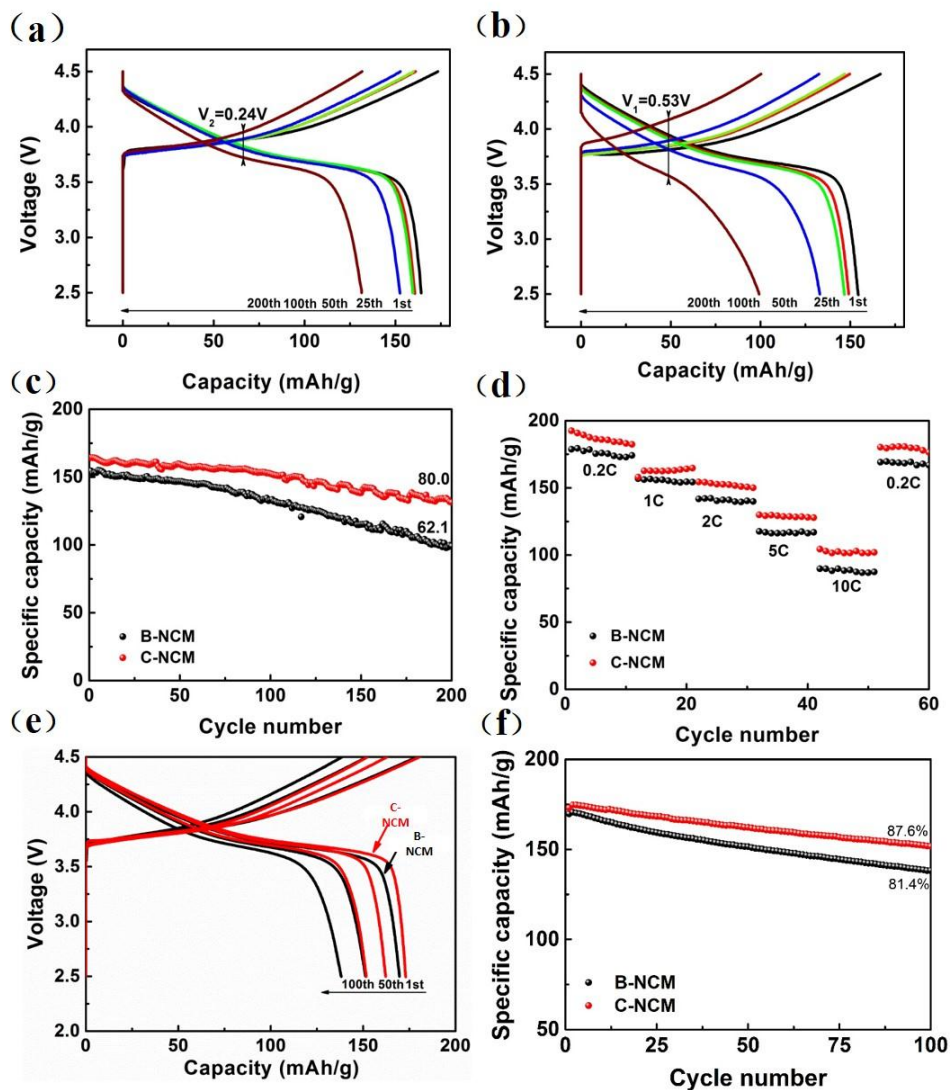
Figure 7. (a, b) Charge-discharge curves of the B-NCM and C-NCM electrodes, respectively. (c) Cycling performance of the B-NCM and C-NCM electrodes at room temperature. (d) Rate capability characteristics. (e) Charge-discharge curves of the B-NCM and C-NCM electrodes at 45 °C. (f) Cycling performance of the B-NCM and C-NCM electrodes at 45 °C.

The electrochemical properties of coin cells were carried out with B-NCM and C-NCM as cathode materials, as shown in Fig. 7. All batteries were firstly cycled at 0.2 C. Fig. 7(a, b) show the charge-discharge profiles of the B-NCM and C-NCM samples with cycles at 1 C. The charge and discharge profiles of both samples are smooth indicating that the electrode structures remain relatively stable under the examined voltage range. In addition, the voltage profiles suggest that the B-NCM

sample has a larger overpotential compared to C-NCM. As shown in Fig. 7, the charge and discharge overpotential of the B-NCM electrode at the 200th cycle is 0.55 V, which is obviously larger than that of the C-NCM electrode with a lower value of 0.24 V. The smaller polarization of C-NCM may be attributed to the smaller charge transfer resistance and more efficient Li-ion transport [19]. This demonstrates that the Li_2SiO_3 layers can effectively protect the NCM from side reactions with electrolyte during cycling [3, 16].

As shown in Fig. 7c, the C-NCM cathode delivers an initial specific capacity of 164.2 mAh g^{-1}, which gradually decreases to 131.4 mAh g^{-1} after 200 cycles at 1 C, (~80.0 % capacity retention), indicating its good reversibility. In comparison, the specific capacity of the B-NCM electrode decreases from 154.5 to 99.2 mAh g^{-1}, corresponding to a capacity loss of 37.9 %. The superior capacity retention of C-NCM cathode may be attributed to the fact that Li_2SiO_3 coating layer can effectively reduce the side reactions between the NCM and the electrolyte and prevent the dissolution of NCM particles at a high voltage of 4.5 V.

Rates performance tests from 0.2 C to 10 C were carried out, as presented in Fig.7d. At 0.2 C, the C-NCM electrode delivers a specific capacity of 192.5 mAh g^{-1}, which is larger than 178.7 mAh g^{-1} of the B-NCM electrode. As the rate is increased from 2 C to 10 C, the specific capacity decreases from 154.4 to 104.4 mAh g^{-1} for the C-NCM electrode. This is a much better rate performance than that of the B-NCM electrode, which only achieves specific capacities of 141.8 and 89.8 mAh g^{-1} at 2 C and 10 C, respectively. The superior rate performance of C-NCM can be ascribed to the improved structural stability and improved diffusion paths for lithium ions.

Table 1. Charge capacity and capacity retention of NCM samples at 1 C

Temperature	Sample	Discharge capacity (mAhg^{-1})		Capacity retention (%)
		First cycle	Last cycle	
Room temperature	B-NCM	154.5	99.2 (200th)	62.1
	C-NCM	164.2	131.4 (200th)	80.0
45℃	B-NCM	169.7	138.2 (100th)	81.4
	C-NCM	173.1	151.7 (100th)	87.6

To investigate the cycling stability of the B-NCM and C-NCM materials at an elevated temperature, the cells were tested at a rate of 1 C for 100 cycles at 45 °C, as shown in Fig. 7(e, f). The discharge capacities of both samples increased to 169.7 and 173.1 mAh g^{-1} at 45 °C compared with 154.5 and 164.2 mAh g^{-1} at room temperature due to the enhanced kinetics of Li^+ migration at a higher temperature. The discharge capacity of the C-NCM sample decreased to 151.7 mAh g^{-1} after 100 cycles, which was 87.6 % of the first discharge capacity. In comparison, the capacity of the B-NCM sample decreased to 138.2 mAh g^{-1} after 100 cycles with 81.4 % capacity retention. These results

demonstrate that Li_2SiO_3 coating layer can greatly improve the electrochemical performance of NCM at elevated temperatures. This is mainly because the layered structure of the Li_2SiO_3-coating layer which can be well-maintained at elevated temperatures. Therefore, this coating layer can effectively suppress the interfacial reaction between the cathode and electrolyte at a high voltage and reduce the interface charge resistance as reported previously [3, 11, 16, 25].

In Fig.8a, the CV curves of both B-NCM and C-NCM exhibit two distinct redox peaks pair between 3.6 and 4.0 V corresponding to the chemical valence change of Ni^{2+}/Ni^{4+} couple [16]. The smaller potential interval of the C-NCM (0.23 V) compared with the 0.27 V of the B-NCM sample indicates smaller electrode polarization [26], which coincides with the charge-discharge profile shown in Fig.7 (a, b). It is noteworthy that the curve of C-NCM sample has a sharper peak and a larger peak current reflects a higher electrochemical redox reaction activity [27, 28]. This suggests that the Li_2SiO_3 coating layer could greatly decrease the electrode polarization and enhance the electrochemical performance of NCM electrode.
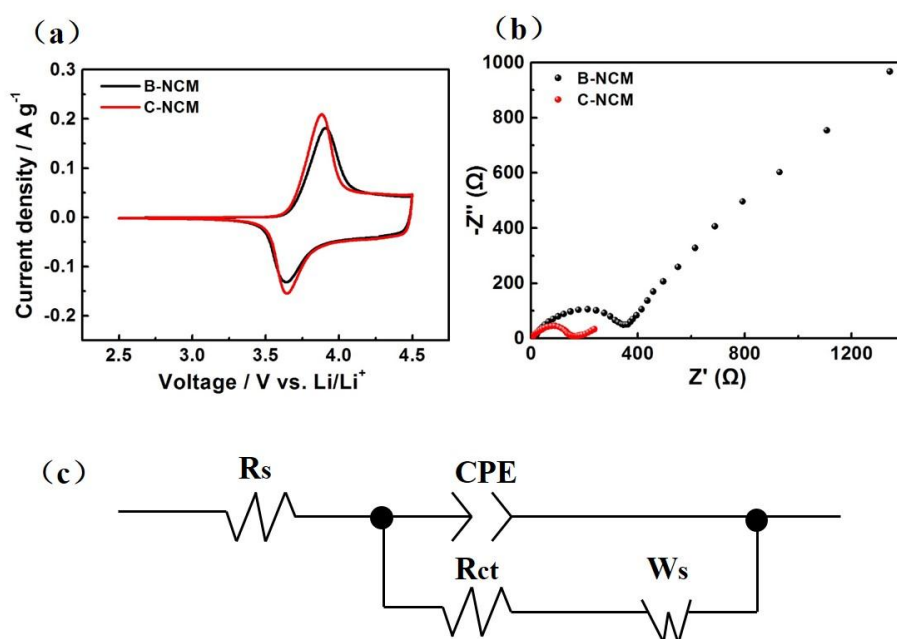
Figure 8. (a) Cyclic voltammetry curves of the B-NCM and C-NCM electrodes at a scan rate of 0.1 mV s^{-1}. (b) Nyquist plots of the B-NCM and C-NCM electrodes after cycles at 1 C. (c) The equivalent circuit used to simulate the EIS data.

Table 2. The simulated values of R_s and R_{ct} from EIS data

Sample	$R_s(\Omega)$	$R_{ct}(\Omega)$
B-NCM	14.9	317.6
C-NCM	3.8	145.3

To further explain the superior electrochemical performance of the C-NCM, EIS measurements were carried out as shown in Fig. 8b. In the Nyquist plot, the diameter of the high frequency semicircle is related to the charge transfer resistance (R_{ct}) between the electrode and electrolyte interface and the low frequency oblique line stands for the ability of lithium-ions to diffuse through the solid electrode. The semicircle that represents the resistance of surface film was not observed probably due to the very small resistance of Li ions transported through surface [3, 16, 29]. As evident from Fig. 8d, the radius of C-NCM electrode is much smaller than that of B-NCM and the simulated values of R_s (related to the resistance of electrolyte solution) and R_{ct} are obtained from an equivalent circuit (Fig. 8c). The C-NCM sample has a rather smaller R_{ct} value (145.3 Ω) than that of B-NCM (317.6 Ω), which contributes to the highly enhanced rate and cycling performance of C-NCM. It can be deduced that the Li_2SiO_3 coating layer can effectively suppress the detrimental interface reactions and protect against cathode dissolution during long cycling.

4. CONCLUSIONS

Li_2SiO_3-coated $LiNi_{1/3}Co_{1/3}Mn_{1/3}O_2$ cathode material been synthesized via a novel and mild method. The existence of the Li_2SiO_3 coating layer was successfully confirmed through a series of characterization techniques such as XPS, FTIR, Raman spectroscopy, HRTEM and EDS. The morphology of NCM did not drastically change after the surface coating and the layered structure of the NCM was well-maintained with less cation mixing ensuring the achievement of good electrochemical performance at a high voltage of 4.5 V. The Li_2SiO_3 coated NCM cathode exhibits a capacity retention of 80.0 % after 200 cycles at room temperature and 87.6 % after 100 cycles at 45 °C, while the corresponding values of bare NCM are only 62.1 % and 81.4 %, respectively. In addition, the discharge specific capacities of Li_2SiO_3 coated NCM cathode at 2 C and 10 C could reach 154.4 and 104.4 mAh g^{-1} compared with the bare NCM with a lower specific capacities of 141.8 and 89.8 mAh g^{-1}, respectively. The enhanced cycling life and rate capability of Li_2SiO_3 coated NCM at both room and elevated temperatures was attributed to the improved Li$^+$ diffusion paths and the reduced charge transfer resistance. Thus, Li_2SiO_3 coating in cathode can offer significant improvement in the electrochemical performance of NCM, particularly under harsh environments.

References

1. E. Y. Zhao, X. F. Liu, Z. B. Hu, L. M. Sun, X. L. Xiao, *J. Power Sources*, 294 (2015) 141.

2. X. Z. Zheng, T. Huang, Y. Pan, W. G. Wang, G. H. Fang, M. X. Wu, *J. Power Sources*, 293 (2015) 196.
3. Y. P. Chen, Y. Zhang, B. J. Chen, Z. Y. Wang, C. Lu, *J. Power Sources*, 256 (2014) 20.
4. F. Fu, G. L. Xu, Q. Wang, Y. P. Deng, X. Li, J. T. Li, L. Huang, S. G. Sun, *J. Mater. Chem.*, 1 (2013) 3860.
5. H. L. Chen, C. P. Grey, *Adv. Mater.*, 20 (2008) 2206.
6. W. B. Hua, X. D. Guo, Z. Zheng, Y. J. Wang, B. H. Zhong, B. Z. Fang, J. Z. Wang, S. L. Chou, H. Liu, *J. Power Sources*, 275 (2015) 200.
7. J. L. Li, C. B. Cao, X. Y. Xu, Y. Q. Zhu, R. M. Yao, *J. Mater. Chem.*, 1 (2013) 11848.
8. W. H. Ryu, S. J. Lim, W. K. Kim, H. S. Kwon, *J. Power Sources*, 257 (2014) 186.
9. Z. H. Yang, J. B. Lu, D. C. Bian, W. X. Zhang, X. N. Yang, J. F. Xia, G. D. Chen, H. Y. Gu, G. Ma, *J. Power Sources*, 272 (2014) 144.
10. N. T. Wu, H. Wu, W. Yuan, S. J. Liu, J. Y. Liao, Y. Zhang, *J. Mater. Chem.*, 3 (2015) 13648.
11. J. L. Li, R. M. Yao, C. B. Cao, *ACS Appl. Mater. Inter.*, 6 (2014) 5075.
12. G. Z. Wei, X. Lu, F. S. Ke, L. Huang, J. T. Li, Z. X. Wang, Z. Y. Zhou, S. G. Sun, *Adv. Mater.*, 22 (2010) 4364.
13. F. Fu, Y. Y. Huang, P. Wu, Y. K. Bu, Y. B. Wang, J. N. Yao, *J. Alloys Compd.*, 618 (2015) 673.
14. H. Kim, M. G. Kim, H. Y. Jeong, H. Nam, J. Cho, *Nano lett.*, 15 (2015) 2111.
15. W. Liu, M. Wang, X. L. Gao, W. D. Zhang, J. T. Chen, H. H. Zhou, X. X. Zhang, *J. Alloys Compd.*, 543 (2012) 181.
16. K. Liu, G. L. Yang, Y. Dong, T. Shi, L. Chen, *J. Power Sources*, 281 (2015) 370.
17. Y. T. Zhang, P. Y. Hou, E. L Zhou, X. X. Shi, X. Q. Wang, D. W. Song, J. Guo, L. Q. Zhang, *J. Power Sources*, 292 (2015) 58.
18. R. Guo, P. F. Shi, X. Q. Cheng, C. Y. Du, *J. Alloys Compd.*, 473 (2009) 53.
19. E. Y. Zhao, X. F. Liu, H. Zhao, X. L. Xiao, Z. B. Hu, *Chem. Commun.*, 51 (2015) 9093.
20. K. Yin, W. M. Fang, B. H. Zhong, X. D. Guo, Y. Tang, X. Nie, *Electrochim. Acta*, 85 (2012) 99.
21. X. Y. Jiang, Y. J. Sha, R. Cai, Z. P. Shao, *J. Mater. Chem.*, 3 (2015) 10536.
22. J. Y. Bai, Z. L. Gong, D. P. Lv, Y. X. Li, H. Zou, Y. Yang, *J. Mater. Chem.*, 22 (2012) 12128.
23. J. I. Lee, Y. Ko, M. Shin, H. K. Song, N. S. Choi, M. G. Kim, S. Park, *Energ. Environ. Sci.*, 8 (2015) 2075.
24. S. K. Martha, H. Sclar, Z. S. Framowitz, D. Kovacheva, N. Saliyski, Y. Gofer, P. Sharon, E. Golikc, B. Markovsky, D. Aurbach, *J. Power Sources*, 189 (2015) 248.
25. R. Guo, P. F. Shi, X. Q. Cheng, L. Sun, *Electrochimi. Acta*, 54 (2009) 5796.
26. C. H. Lin, Y. Z. Zhang, L. Chen, Y. Lei, J. K. Ou, Y. Guo, H. Y. Yuan, D. Xiao, *J. Power Sources*, 280 (2015) 263.
27. J. H. Park, J. H. Cho, S. B. Kim, W. S. Kim, S. Y. Lee, S. Y. Lee, *J. Mater. Chem.*, 22 (2012) 12574.
28. Z. D. Huang, X. M. Liu, S. W. Oh, B. Zhang, P. C. Ma, J. K. Kim, *J. Mater. Chem.*, 21 (2011) 10777.
29. D. W. Xu, Y. B. He, X. D. Chu, Z. J. Ding, B. H. Li, J. F. He, H. D. Du, X. Y. Qin, F. Y. Kang, *ChemSusChem*, 8 (2015) 1009.